ACS OMEGA

Open Access

http://pubs.acs.org/journal/acsodf

Article

Theoretical Design of New Grafted Molecules D-Glucosamine-Oxyresveratrol-Essential Amino Acids: DFT Evaluation of the Structure−Antioxidant Activity

Salima Hamadouche, Hafida Merouani, Omaima Aidat, Nadia Ouddai, Barbara Ernst, Manawwer Alam, and Yacine Benguerba*

Cite This: *ACS Omega* 2024, 9, 37128−37140

Read Online

ACCESS | Metrics & More | Article Recommendations

ABSTRACT: In the pursuit of innovative high-performance materials suitable for antioxidant applications, the density functional theory was employed to design a series of compounds derived from small biodegradable organic molecules. This study involved grafting the negatively charged unit D-glucosamine (GleN) and essential amino acids onto the 3 and 4' carbons of the backbone of *trans*-2,4,3′,5′-tetrahydroxystilbene (*trans*-OXY), respectively. The aim was to prevent *trans*-OXY degradation into the *cis* region and enhance its electronic and antioxidant properties. Theoretical calculations using DFT/PW91/TZP in water revealed that the designed biomolecules (GleN-OXY-AA) outperformed both free OXY units and essential amino acids in terms of antioxidant efficacy, as indicated by the bond dissociation energy (BDE) findings. Notably, GleN-OXY-Ile and GleN-OXY-Trp compounds exhibited an average BDE of 66.355 kcal/mol, translating to 1.82 times the activity of *t*-OXY and 1.55 times the action of ascorbic acid (Vit C). AIM analysis demonstrated that the proposed biomaterials favored the formation of quasi-rings through intramolecular H···O hydrogen bonds, promoting π-electron delocalization and stabilization of radical, cationic, and anionic forms. Quantum calculations revealed the release of hydrogen atoms or electrons from sites of reduced electronegativity, visually identified by MEP maps and estimated by Hirshfeld atomic charges.

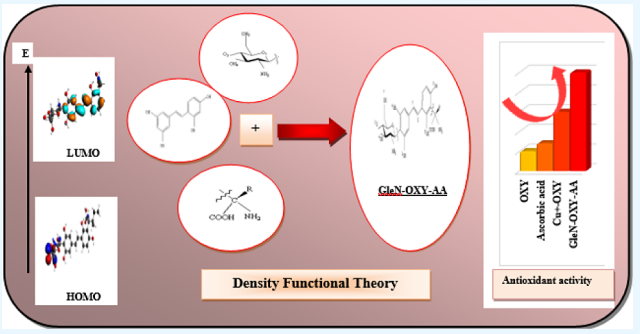

1. INTRODUCTION

Polyphenols (PP) are inherently unstable substances, and their health impact largely hinges on the consumption levels and bioavailability, which can limit their effectiveness in vivo.[1−3] During food processing, preserving the bioactivity of PP becomes critical due to its sensitivity to factors like oxygen, temperature, pH, light, and the conditions of the gastrointestinal tract. The antioxidant efficacy of polyphenols diminishes notably when exposed to pH levels above 7, such as those typically encountered in the human digestive tract with a pH around 8.[4−7]

Oxyresveratrol (2,4,3′,5′-tetrahydroxystilbene; OXY) is a polyphenolic compound derived from plants,[8,9] notably extracted from the heartwood of *Artocarpus lacucha* Roxb,[10] or mulberry wood (*Morus alba* L.).[9] Due to its simple chemical structure and broad therapeutic potential,[9,11−16] OXY has attracted considerable interest. However, its weak solubility, limited bioavailability, and stability issues constrain its pharmacological applications.[17] Studies indicate that the *trans* isomer of OXY exhibits significantly higher antioxidant activity than its *cis* counterpart.[9,18] In our previous study,[19] we demonstrated that the antioxidant efficiency of *trans*-OXY (*t*-OXY) is markedly enhanced when it forms complexes with copper metal cations compared to its *cis* form. Nevertheless, like all stilbenes, OXY is highly photosensitive and undergoes rapid degradation when exposed to UV radiation,[20] high temperatures, alkaline pH, or enzymatic environments.[21] Chemical degradation often involves isomerization from the *trans* to the *cis* structure, requiring minimal energy of approximately 20 kcal/mol.[22] Over the past decade, various techniques have been proposed to address these challenges, including cyclodextrin-complexation, emulsion, liposomes, solid−lipid nanoparticles, polymer nanoparticles, encapsulation, and assembly.[23−28]

The development of biomaterials involves assembling small, biocompatible molecules through rational design to harness

Received: May 7, 2024
Revised: July 28, 2024
Accepted: August 6, 2024
Published: August 20, 2024

their activities, promising significant advancements in therapeutic applications.[29] When designing small molecules for therapy, it is crucial to consider units that are both biodegradable and bioactive, such as sugars, amino acids, or nucleic acids, which degrade into harmless metabolites over time, forming a broad foundation for developing new substances.[30,31]

For this investigation, essential amino acids (AA), the indispensable AA, are employed as assembly units with *t*-OXY.[32] These include valine (Val), leucine (Leu), isoleucine (Ile), threonine (Thr), methionine (Met), phenylalanine (Phe), tryptophan (Trp), and histidine (His). Numerous studies have highlighted the benefits of AA, particularly its antioxidant activity,[33,34] particularly antioxidant activity.[35−39] According to the World Health Organization (WHO), "sugar" refers to all monosaccharides and disaccharides added to nutrition.[40] Excessive consumption of sugars has been linked to increased risks of cardiovascular diseases, diabetes,[41] and particularly cancer by promoting Fenton reaction in vivo and oxidative stress.[42] To mitigate these risks, we opted for D-glucosamine, a chitosan monomer whose chair conformation resembles that of glucose.

Glucosamine residues (GleN) are fundamental components of chitosan, commonly sourced from crustacean skeletons, and the second most abundant polymer after cellulose. GleN is known for its diverse biological, nutritional, and pharmaceutical effects, including membrane stabilization, liver protection,[43] promotion of wound healing,[44] and potential for osteoporosis treatment.[45] Due to its renewable nature and excellent properties, GleN is gaining attention for its simple absorption and remarkable biocompatibility.[46] D-glucosamine is recognized for its significant antioxidant activity[47−50] and its ability to chelate metal ions.[51,52] This property gives it secondary antiradical activity. Due to the diverse biological activity of this particular polymer, its exceptional biocompatibility, complete biodegradability, and low toxicity combined with its extremely complex functionalities, an original category of physiological substance with highly sophisticated functions has developed.[53−55] Attempts are being made to modify these adaptable polysaccharides to take advantage of their particular qualities and maximize their potential.[56,57]

Grafting is an intriguing approach for introducing functional groups or small molecules into polymers or monomers,[58] creating new compounds with tailored properties for specific applications.[59] Recently, there has been growing interest in grafting antioxidant molecules onto polymer chains or monomers,[60] enhancing their bioactivities compared to free phenolic compounds, particularly regarding antioxidant efficacy.[61−64] These grafted polymers exhibit novel qualities, such as improved mechanical and physiological properties and altered solubility.[65,66]

This study focuses on stabilizing the *trans*-OXY configuration and preventing its conversion to *cis*-OXY to maximize its powerful antioxidant properties. To achieve this objective, we grafted a chitosan molecule, specifically negatively charged D-glucosamine. Previous experimental findings have demonstrated that compounds with higher basicity exhibit superior antioxidant activity compared to L-ascorbic acid,[67] which aligns with our earlier research.[19] Additionally, by incorporating an essential amino acid, we aim to investigate how these grafts influence the stability of *trans*-OXY and enhance the antioxidant capacity of these innovative biomaterials.

Subsequently, we formulated a composite of three components, as illustrated in Figure 1. Fragment I includes a

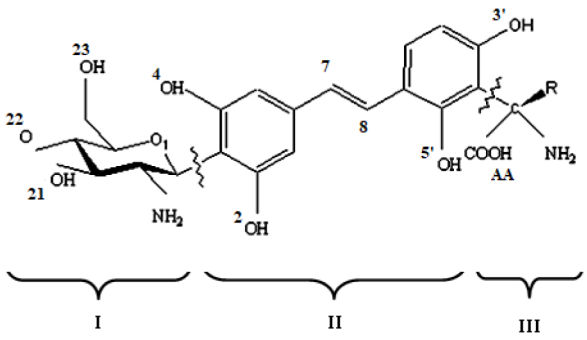

Figure 1. Illustration of the model of chemical structures of the new biomaterials.

negatively charged D-glucosamine group at position O5 to ensure water solubility.[68] Fragment II comprises OXY, while fragment III integrates the essential amino acid.

2. COMPUTATIONAL DESCRIPTIONS

Amsterdam Density Functional (ADF) software package[69] was used to optimize all the biomaterial structures in this work using density functional theory (DFT),[70] including single-point calculations. The PW91 level (Perdew−Wang (1991)),[71] the exchange−correlation function GGA (generalized gradient approximation) functional, and the slater TZP (triple-ζ polarized) set of atomic bases are the valence orbitals of all atoms (1*s* for H; 2*p* for O, C, and N; and 3*p* for S).[72] Internal orbitals were retained with frozen cores. Becke is the integration algorithm, and 10^{-3} a.u. is the energy convergence criteria. The impact of solvents is taken into consideration by the conductor-like screening model (COSMO),[73] with the dielectric constant of water (ε = 78.4) and van der Waals radii 1.93 Å. The program's graphical interface was utilized to build the structure for the computations, as the biomaterials lack an X-ray structure. Furthermore, to attain computing precision, it was established that all the optimized structures reached the imaginary zero frequency, which marked the global minima of the potential energy surface.

2.1. Antioxidant Activity Descriptors. The dissociation energy of intramolecular homolytic cleavage of the chemical bonds between O and H, found in the compounds under study, determines the antioxidant activity. The ADF code can supply this energy by performing the following actions:

— Perform a DFT calculation on each of the two fragments of the molecule: ArO radical and H atom present in all sites.

— Intermolecular interactions are grouped according to their specific energy, and the bond dissociation energy is computed using the formula:

$$BDE(E0) = E_{elect} + E_{Pauli} + E_{orb} = E_{elect} + E_{Pauli+orb} \quad (1)$$

where E_{elect}: The electrostatic energy employed in qualifying the electrostatic interaction between the two sections. E_{pauli}: Pauli energy, a destabilizing component associated with repulsive interactions between pieces. E_{orb}: The orbital interaction can be defined in the framework of the single electronic approximation as the sum of the stabilizing interactions with two electrons and two orbitals. The

https://doi.org/10.1021/acsomega.4c04356
ACS Omega 2024, 9, 37128−37140

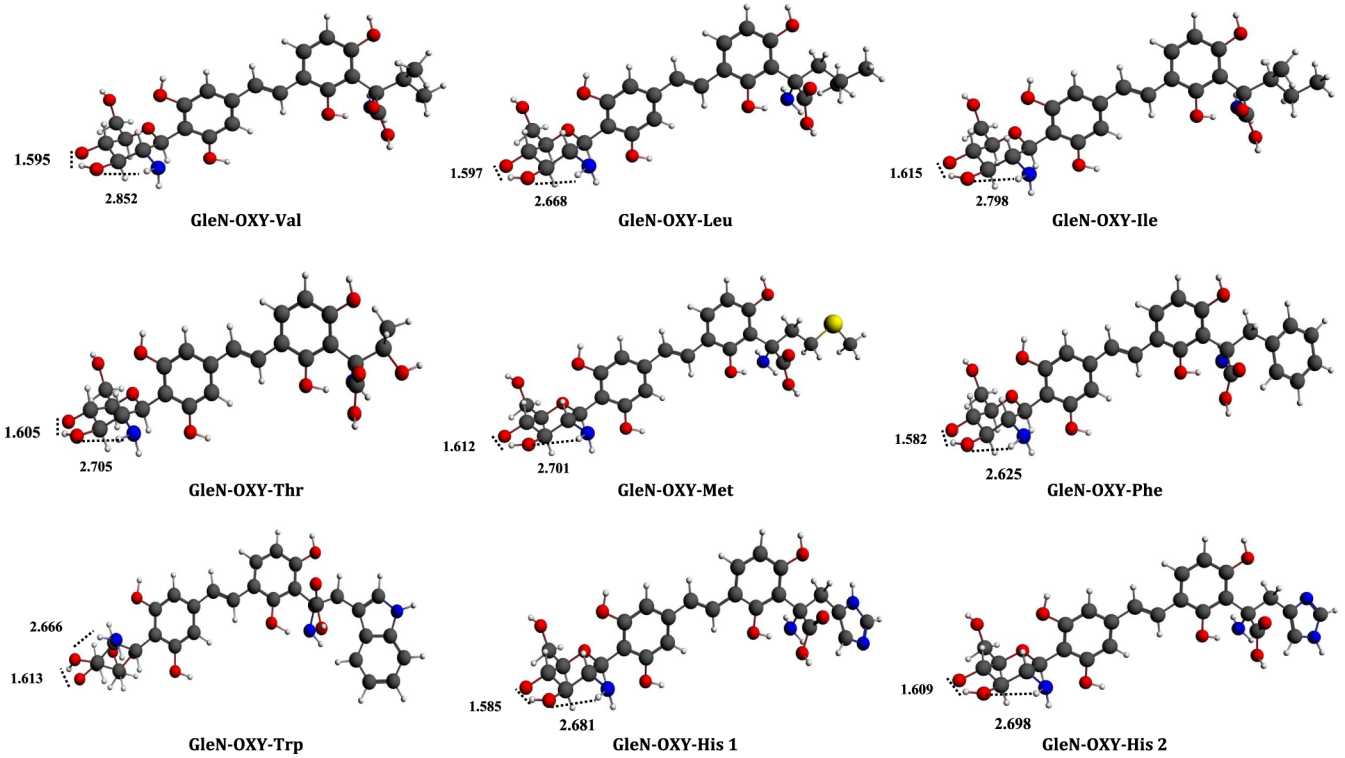

Figure 2. Optimized structures using the DFT/PW91/TZP/water level of theory of grafted OXY with GleN and essential amino acids and GleN's hydrogen bonds length in (Å).

Table 1. Bond Lengths (Å) for the Target Compounds Optimized in Water at the PW91/TZP Level of Theory

	bond distances (Å)											
compounds	$C_7{=}C_8$	$C_7{-}C_6$	$C_8{-}C_{6'}$	$C_1{-}C_2$	$C_2{-}C_3$	$C_3{-}C_4$	$C_4{-}C_5$	$C_5{-}C_6$	$C_5{-}C_6$	$C_{1'}{-}C_{2'}$	$C_{2''}{-}C_{3'}$	ref
t-OXY	1.346	1.446	1.440	1.398	1.385	1.390	1.386	1.389	1.397	1.398	1.378	18
GleN-OXY-Val	1.346	1.444	1.438	1.397	1.385	1.399	1.397	1.388	1.395	1.397	1.374	
GleN-OXY-Leu	1.346	1.444	1.437	1.397	1.385	1.400	1.397	1.388	1.396	1.395	1.374	
GleN-OXY-Ile	1.346	1.444	1.437	1.397	1.385	1.398	1.396	1.388	1.395	1.397	1.374	
GleN-OXY-Thr	1.346	1.443	1.438	1.397	1.385	1.399	1.396	1.387	1.395	1.395	1.374	
GleN-OXY-Met	1.346	1.444	1.438	1.397	1.385	1.399	1.396	1.388	1.395	1.396	1.374	
GleN-OXY-Phe	1.347	1.444	1.439	1.397	1.385	1.400	1.396	1.388	1.396	1.394	1.373	
GleN-OXY-Trp	1.347	1.446	1.436	1.398	1.383	1.403	1.397	1.390	1.397	1.395	1.375	
GleN-OXY-His 1	1.347	1.446	1.437	1.397	1.384	1.399	1.396	1.389	1.395	1.394	1.375	
GleN-OXY-His 2	1.347	1.445	1.439	1.396	1.386	1.399	1.397	1.388	1.396	1.396	1.374	

	bond distances (Å)											
compounds	$C_{3'}{-}C_{4'}$	$C_{4'}{-}C_{5'}$	$C_{5'}{-}C_{6'}$	$C_1{-}C_2$	$O_{5'}{-}H_{5'}$	$O_{3'}{-}H_{3'}$	$O_2{-}H_2$	$O_4{-}H_4$	$O_{AA}{-}H_{AA}$	$O_{CH7}{-}H_{CH7}$	$O_{CH4}{-}H_{CH4}$	ref
t-OXY	1.395	1.385	1.385	1.407	0.980	0.980	0.980	0.980	—	—	—	18
GleN-OXY-Val	1.399	1.398	1.413	1.406	1.083	0.981	0.980	0.981	0.988	0.980	1.053	
GleN-OXY-Leu	1.398	1.396	1.416	1.410	1.093	0.981	0.980	0.980	0.988	0.977	1.057	
GleN-OXY-Ile	1.400	1.395	1.414	1.406	1.097	0.980	0.981	0.980	0.987	0.975	1.051	
GleN-OXY-Thr	1.396	1.395	1.417	1.412	1.094	0.981	0.979	0.980	0.987	0.976	1.055	
GleN-OXY-Met	1.397	1.395	1.414	1.409	1.086	0.981	0.980	0.981	0.990	0.979	1.052	
GleN-OXY-Phe	1.396	1.397	1.418	1.411	1.076	0.981	0.980	0.980	0.990	0.975	1.059	
GleN-OXY-Trp	1.398	1.397	1.418	1.412	1.100	0.981	0.980	0.981	0.988	0.977	1.052	
GleN-OXY-His 1	1.396	1.400	1.420	1.414	1.093	0.981	0.980	0.980	0.989	0.977	1.059	
GleN-OXY-His 2	1.398	1.397	1.416	1.411	1.092	0.982	0.979	0.979	0.991	0.976	1.054	

contribution of (E_{Pauli}) and (E_{orb}) are generally grouped in($E_{Pauli + orb}$).[74]

2.2. Atoms in Molecules Analysis (AIM). Several DFT techniques are available to describe the chemical bond characteristics. Atoms in molecules (AIM) analysis is one such approach. The characteristics computed at the bond critical point (BCP) or the ring critical point (RCP) consist of the following: electronic density $\rho(r)$, Laplacian density $\nabla^2\rho(r)$, potential energy density $V(r)$, kinetic energy density $G(r)$, and total electron energy $H(r)$. These descriptors serve as criteria for assessing the variance in charge density and binding characteristics of the compounds under consideration.

https://doi.org/10.1021/acsomega.4c04356
ACS Omega 2024, 9, 37128−37140

Table 2. Dihedral Angles (deg) for the Target Compounds Optimized at the PW91/TZP Level of Theory in Water

	bond angles			
compounds	α (C_8−$C_{1'}$−$C_{6'}$−C_7)	β (C_7−C_1−C_6−C_8)	θ (O−$C_{3'}$−$C_{4'}$−C_{AA})	ref
t-OXY	2.1	3.0	—	18
GleN-OXY-Val	1.8	3	2.9	
GleN-OXY-Leu	1.5	2.7	0.0	
GleN-OXY-Ile	1.6	2	0.4	
GleN-OXY-Thr	1.4	0.7	3	
GleN-OXY-Met	1.1	0.4	1.0	
GleN-OXY-Phe	0.9	0.5	1.8	
GleN-OXY-Trp	1.6	1.6	2.0	
GleN-OXY-His 1	2.1	1.5	1.0	
GleN-OXY-His 2	2.8	1.6	1.0	

The Bader's AIM method gives a topological analysis of a molecule's chemical bonds.75 The presence of a critical point in the AIM analysis allows for the characterization of a chemical bond. The electron density at the critical point provides details about a bond's characteristics. The AIM technique provides useful tools for investigating the structure's π-electron delocalization qualities regarding the electron density parameters determined at the RCP.76 Using ADF's t21 file, topological analysis was carried out with DGrid and ADF.77

3. RESULTS AND DISCUSSION

3.1. Structure-Antioxidant Activity Correlations and Molecular Structures. The GleN-OXY-AA model was built based on previous models of stilbenes with a prenyl moiety on carbons 3 and 4'.[78−80] In our investigation, we chose to substitute the chitosan monomer (GleN) on cycle A with an amino acid on cycle B. The GleN monomer, which has a negative charge on the oxygen atom O5, is grafted as a functionalized molecule on the atom of OXY. The amino acids were individually attached to stilbene by the carbon carrying the carboxyl and amine functions (see Figure 2).

DFT calculations were performed on GleN-OXY-AA models. To our knowledge, none has been synthesized. Our choice is not arbitrary; negatively charged GleN chitosan grafts and essential amino acids increase the steric effect and hinder the transition to the *cis* isomer. The bond lengths and angles (geometric parameters) are examined with those of the free parent compounds, oxyresveratrol, the GleN monomer, and the essential AAs before grafting (see Table 1).

The diverse hydrogen bonding characteristics of the GleN molecule are the reason for the relatively large number of conformers. In total, there are more than 50 D-glucosamine conformers.81 The GleN conformer in the grafted molecule was imposed by the intermolecular interactions, which explain the arrangement of atoms and molecules within a chemical system.[82−86] So, first, the minimum energy structures of each grafted GleN-OXY-AA structure were obtained by optimization of each of them separately. These are illustrated in Figure 1, followed by the optimization in a free state of selected negatively charged GleN conformers and the structure of essential amino acids, in equilibrium for comparison.

The chair-shaped structure of GleN is constructed by hydroxyls and amine groups on the molecular chain, promoting the appearance of intramolecular and intermolecular hydrogen bonds.[87,88] The conformation obtained for the GleN monomer structure is stabilized by forming the two intramolecular hydrogen bonds (Figure 1). A hydrogen bond is formed by the attraction of a covalent donor pair *X* and a hydrogen atom H, so the H is attached to a more electronegative acceptor *X* (ion or molecule).89 Hydrogen bonds occur in the structures examined between the H atoms of hydroxyl groups (−OH) and neighboring O atoms, explaining the elongation of the hydroxyl group in O_{CH2}−fH_{CH2}, which varies from 1.051 to 1.059 Å, or between the H atoms of the amine groups (−NH2). The shortest distance between O−H···O measures between 1.582 and 1.615 Å, while the lengths of N−H···O range from 2.625 to 2.852 Å, respectively, as shown in Figure 1. Additionally, according to these data, the average lengths between O−H···O are less than 1.8 Å. And the lengths of N−H···O are larger than 2.0 Å. These data were classified as strong hydrogen bonds for the former and weak for the latter.82 We also note that the O_{CH4}−H_{CH4} bond on GleN varies from 1.052 to 1.057 Å.

A priori, the grafted OXY retains the property of the double bond of the ethylenic bridge identified in column C_7=C_8, which is distinctive to the stilbene structure in all the compounds investigated. C_7−C_6 and C_8−$C_{6'}$ bond lengths vary from the OXY by 0.003 and 0.004 Å, respectively. The electrical resonance in the two aromatic rings, A and B, can be observed by the bond lengths in each of the rings present in the grafted OXY, which are roughly 1.4 Å. The length of the $O_{5'}$−$H_{5'}$ bond is 1.100 Å, relatively longer than the lengths of the $O_{3'}$−$H_{3'}$, the length of the O_2−H_2, and the length of the O_4−H_4 bonds (0.980 Å) (see Table 1). The bond length is related to the type and order of the interaction,90 designating this site as the most active in the molecule. For the essential amino acids, our interest focused on the ends of the carboxylic functional group and, more precisely, on O−H, which neighbors the atom of the OXY fragment. To highlight the influence of the grafting of the latter on the geometric configuration. The O−H bond shows alterations in terms of length from approximately 0.007 to 0.011 Å.[91−97]

Because the structure's planarity facilitates electron delocalization, it plays a key role in antioxidant properties.98 Given that the monomer GleN is twisted in all structures, only the OXY angles from the AA to the OXY will be considered (O−$C_{3'}$−$C_{4'}$−C_{AA}) (Table 2). The modifications observed at the levels of the angles (C_7−C_1−C_6−C_8) and (C_8−$C_{1'}$−$C_{6'}$−C_7) of the OXY after grafting highlight the relationship between grafting and structural planarity, where the angle α goes from 2.1° to 0.9° and the angle β is from 3.0° to 0.4°. However, angle θ shows the most interesting variation of 0.0°. Thanks to the ethylene bridge that joins the aromatic ring and the existence of the carboxylic acid function, the compounds investigated have a nearly planar structure, which considerably

https://doi.org/10.1021/acsomega.4c04356
ACS Omega 2024, 9, 37128−37140

Table 3. O−H Bond Homolytic Dissociation Energies Using BDE (E0) Fragmentation Analysis in (kcal/mol) of all Geometries with All Amino Acids Estimated Using DFT PW91/TZP Level of Theory in Water Solvent are Reported at 298.15K

BDE (E_0) (kcal/mol)												
GleN-OXY-AA												
		AA before-assembly		GleN		OXY				AA after-assembly		ref
compounds	OH	OH_{AA}		11-OH	13-OH	5′−OH	3′−OH	2-OH	4-OH	OH_{AA}		
Ascorbic acid	**103.33**	—	—	—	—	—	—	—	—	—	—	
t-OXY	—	—	—	—	—	122.16	121.26	130.87	129.83	—	—	18
GleN-OXY-Val	—	166.03	—	135.83	145.23	87.64	67.33	85.11	112.69	71.78	—	
GleN-OXY-Leu	—	148.01	—	136.79	146.45	90.71	69.64	84.60	111.73	70.88	—	
GleN-OXY-Ile	—	154.15	—	135.79	145.13	86.34	**66.34**	83.91	110.32	69.76	—	
GleN-OXY-Thr	—	144.87	222.53	124.16	147.57	94.02	68.24	86.35	112.32	76.60	127.96	
GleN-OXY-Met	—	135.63	—	118.67	136.53	89.49	69.26	84.52	95.13	69.14	—	
GleN-OXY-Phe	—	167.62	—	125.31	138.29	91.66	70.32	87.35	115.65	72.43	—	
GleN-OXY-Trp	—	137.56	—	135.21	144.98	87.58	**66.37**	83.41	111.19	69.92	—	
GleN-OXY-His 1	—	136.91	—	124.19	146.30	91.22	66.55	85.25	91.36	72.57	—	
GleN-OXY-His 2	—	137.37	—	122.78	145.21	89.85	69.29	84.38	89.48	69.15	—	

promotes delocalization.[99] The latter is positioned in the molecule to obtain the most stable structure. The carboxylic functionality is arranged such that the hydrogen of the hydroxyl group is oriented in a *cis* configuration relative to the oxygen atom of the carbonyl group.[98]

3.2. Antioxidant Activity Descriptors. *3.2.1. Fragmentation by BDE (E0) of the O−H Bonds.* The BDE (E0) parameter approach was acquired by performing a single-point calculation using PW91/TZP on the optimized structures to calculate the reported dissociation energy data. ArO and H are the two fragments created from each molecule. The COSMO model was used in an aqueous medium (see Table 3).

The homolytic dissociation energy BDE (E0) represents a reliable parameter to describe the mechanism, which involves the transfer of a hydrogen atom from a hydroxyl group of the antioxidant molecule to the free radical. The weakest O−H bond (lowest BDE (E0)) should lead to the most likely reaction and the most significant antioxidant activity. The data in Table 3 show that the antioxidant activity of all grafted biomaterials is significantly improved compared to the activity of ascorbic acid and even twice as much as that of free OXY.

The antioxidant activity of the grafted OXY was significantly boosted following the binding of the negatively charged GleN monomer in position 3 and AA in position 4′. This improvement is felt on its four respective sites, and this is true for all of the biomaterials. Hence, they are ideally suited to operate as scavengers, confirming an improvement in the antioxidant activity in the compound model compared to the natural compound (OXY, BDE(E0): 121.26 kcal/mol) .

In all the systems, the site with the lowest energy, BDE (E0) is identified as the optimal antioxidant site. It is always found on the OXY backbone at the 3′−OH position, either before or after grafting. The requirement to promote the delocalization of the unpaired electron after radicalization is the character of the hydroxyl groups directly linked to the compounds' aromatic cycle. Therefore, the results demonstrated that the antioxidant activity is always more effective on the 3′−OH of the B ring of the OXY geometry.

Yet, the system may inhibit reactive species by radicalizing the carboxylic group's hydroxyl. Thus, abstraction of the H atom from such a group (OHAA) was investigated for all compounds. Based on the BDE (E0) energies collected, the effectiveness of the antiradical activity of the amino acids after association with OXY is significantly improved compared to the BDE (E0) energies of the AA before the association (see Table 3). So, for this radicalization, the acidity of the hydrogen atom no longer hinders the transfer of the hydrogen atom as a single entity. Thus, the acid is modeled to reduce the distance between the carboxylic acid function and the aromatic ring.[98,99]

The BDE (E0) energy value of amino acids is ranked directly after the 3′−OH value, which reflects the best site in all structures and even compared to that of OXY, except for the second site in methionine. According to the calculated BDEs, the sites of antiradical activity can be classified as follows:

$$3'\text{-OH} < \text{AA-OH} < \text{2-OH} < 5'\text{-OH} < \text{4-OH} < \text{11-OH} < \text{13-OH}$$

By analyzing the BDE (E0) values, the results reveal the following two compounds: GleN-OXY-Ile and GleN-OXY-Trp have the highest antioxidant activity, with the lowest values of the entire series under study of 66.34 and 66.37 kcal/mol, respectively. Significant differences distinguish the BDE (E0) energies of GleN-OXY-Ile and GleN-OXY-Trp compared to the free parent molecules, and with approximate values of 54.92 kcal/mol for the OXY, 36.99 kcal/mol for ascorbic acid, and 76.01 kcal/mol for free AAs in water. So, 1.82 times compared to the activity of *t*-OXY, even 2.5 times that of free essential AAs, and 1.55 times compared to ascorbic acid (Vit C).

3.2.2. Electronic Properties of GleN-OXY-AA Compounds. Additional insights into the antioxidant activity can be obtained from the energies of the frontier orbitals. According to the energy values indicated in Table 4, all compounds are stable. However, GleN-OXY-Val is the most stable structure with a HOMO/LUMO energy gap of 1.91 eV.

Low-energy HOMO molecules have a low ability to donate electrons. In contrast, the molecule may be a potential electron donor if its HOMO energy is higher.[100,101] The energy gap is correlated to HOMO and LUMO; $E_{(gap)}$ is the absolute energy difference between the frontier molecular orbitals, which indicates the reactivity of the compounds and illustrates that this activity grows as the energy gap decreases.[102] Indeed, upon comparison of GleN-OXY-Ile and GleN-OXY-Trp to the

https://doi.org/10.1021/acsomega.4c04356
ACS Omega 2024, 9, 37128−37140

Table 4. $E_{(gap)}$ (eV), $\sum$ Negative Charges, $\sum$ Positive Charges, $\sum$ of Charges, and Hirshfeld Charge of the $H_{3'}$, $O_{3'}$, H_{AA}, and O_{AA} for the Target Compounds Calculated by Theoretical Level DFT PW91/TZP in Water Solvent at 298.15 K

		GleN			OXY				AA				
compounds	$E_{(gap)}$ (eV)	$\sum$ negative charges	$\sum$ positive charges	$\sum$ of charges	$\sum$ negative charges	$\sum$ positive charges	$\sum$ of charges	$O_{3'}$	$H_{3'}$	$\sum$ negative charges	$\sum$ positive charges	$\sum$ of charges	O_{AA}	H_{AA}	ref
T-OXY	2.51	—	—	—	−1.499	1.499	0.000	−0.182	0.203	—	—	—	—	—	18
GleN-OXY-Val	1.91	−1.631	0.589	−1.042	−1.376	1.232	−0.144	−0.137	0.203	−0.836	1.021	0.185	−0.121	0.214	
GleN-OXY-Leu	1.88	−1.608	0.614	−0.994	−1.399	1.226	−0.173	−0.145	0.201	−0.907	1.129	0.222	−0.120	0.217	
GleN-OXY-Ile	1.82	−1.629	0.593	−1.036	−1.384	1.231	−0.153	−0.137	0.202	−0.907	1.096	0.189	−0.121	0.213	
GleN-OXY-Thr	1.85	−1.631	0.565	−1.066	−1.382	1.234	−0.148	−0.133	0.205	−0.888	1.078	0.190	−0.131	0.214	
GleN-OXY-Met	1.86	−1.631	0.590	−1.041	−1.393	1.232	−0,161	−0.145	0.202	−0.883	1.084	0.201	−0.118	0.220	
GleN-OXY-Phe	1.84	−1.621	0.582	−1.039	−1.377	1.24	−0.137	−0.141	0.203	−0.920	1.103	0.183	−0.120	0.218	
GleN-OXY-Trp	1.83	−1.642	0.589	−1.053	−1.399	1.227	−0.172	−0.144	0.203	−1.081	1.304	0.223	−0.111	0.218	
GleN-OXY-His 1	1.83	−1.631	0.586	−1.045	−1.386	1.236	−0.150	−0.142	0.204	−0.992	1.185	0.193	−0.122	0.218	
GleN-OXY-His 2	1.84	−1.631	0.590	−1.041	−1.388	1.234	−0.154	−0.144	0.203	−0.969	1.167	0.198	−0.114	0.221	

other compounds studied, the movement of electrons from HOMO to LUMO is comparatively more straightforward to achieve if we examine the H−L energy gaps. $E_{(gap)}$ = 1.82 and 1.83 eV correspond well to the lowest values, proving the compounds' maximum reactivity, making them the best electron donor candidates among the compounds studied. This evidence supports the BDE (E0) trend reviewed previously, which indicates that GleN-OXY-Ile and GleN-OXY-Trp are the best antioxidant candidates.

The energies and spatial expansions of the frontier orbitals, namely, HOMO, LUMO, HOMO − 1, and LUMO + 1, are represented for each of the compounds studied in Figure 3. These frontier orbitals tell us about the electron donor/acceptor character and the nature of the fragment responsible for the phenomenon. According to Figure 3, electronic donation is carried out through the GleN fragment. The OXY and amino acid are the electron acceptor fragments (see Figure 3). The predictions given by the theory of frontier orbitals; qualify the structures studied in this manuscript as good acceptors of electrons through OXY fragments and amino acid orbitals.

Hirshfeld's atomic charges (see Table 4) tell us about the mode of connection of the OXY to the rest of the structure. The nature of the variations in charge values between free and complexed OY shows a covalent bond between the amorphous OXY and the rest of the complex (see Table 4). The molecular orbitals visualized in Figure 4 confirm and clarify their nature. Indeed, OXY binds to GleN by a covalent bond and to the amino acid by an ionic bond.

DFT calculated the charge distribution of all compounds; particular interest focused on the OH3′ and OHAA sites due to the BDE(E0) values found to be promising. The antioxidant activity calculated using BDE(E0) is correlated to the charge carried by the oxygen atom. Figure 5 visualizes the curve of the variation of the antioxidant activity as a function of the oxygen charges of the two sites, $OH_{3'}$ and OH_{AA}. The curve obtained with a correlation coefficient (R) equal to 0.96 and 0.98, respectively (see Figure 5). It could be suggested that sites with low negative charges are good donors of electrons and hydrogen atoms to oxidizing agents.[103,104]

3.2.3. Molecular Electrostatic Potentials (MEP). The molecular electrostatic potential is an imaging approach to present the molecule with clouds of graded colors connected to the reactivity of electrophilic and nucleophilic sites.105 The red color describes areas with the greatest negative electrostatic potential (highest density), which is the preferred site for electrophilic attack. Blue are the areas having the lowest density and highest positive electrostatic potential, which is the preferred site for nucleophilic attack. From the MEP plots, the map shows that the distribution of negative potential sites of the molecules is centered only on the oxygen atoms attached to GleN. However, the sites of the positive potentials are located around the hydrogen atoms (H2, H4, H3′, and H5′) of the OXY and (HAA) of the carboxyl group of the amino acid (see Figure 6). Potentially, positive sites play an important role in the donation of hydrogen atoms to oxidizing agents. Based on these findings, it can be asserted that these are the most active sites. This analysis aligns perfectly with our respective results.

3.2.4. Analysis of the Highest Antioxidant Compounds by the AIM Method. The AIM parameters were acquired by "single-point" calculation using geometries optimized with PW91/TZP/water. Table 5 contains the values of the AIM

https://doi.org/10.1021/acsomega.4c04356
ACS Omega 2024, 9, 37128−37140

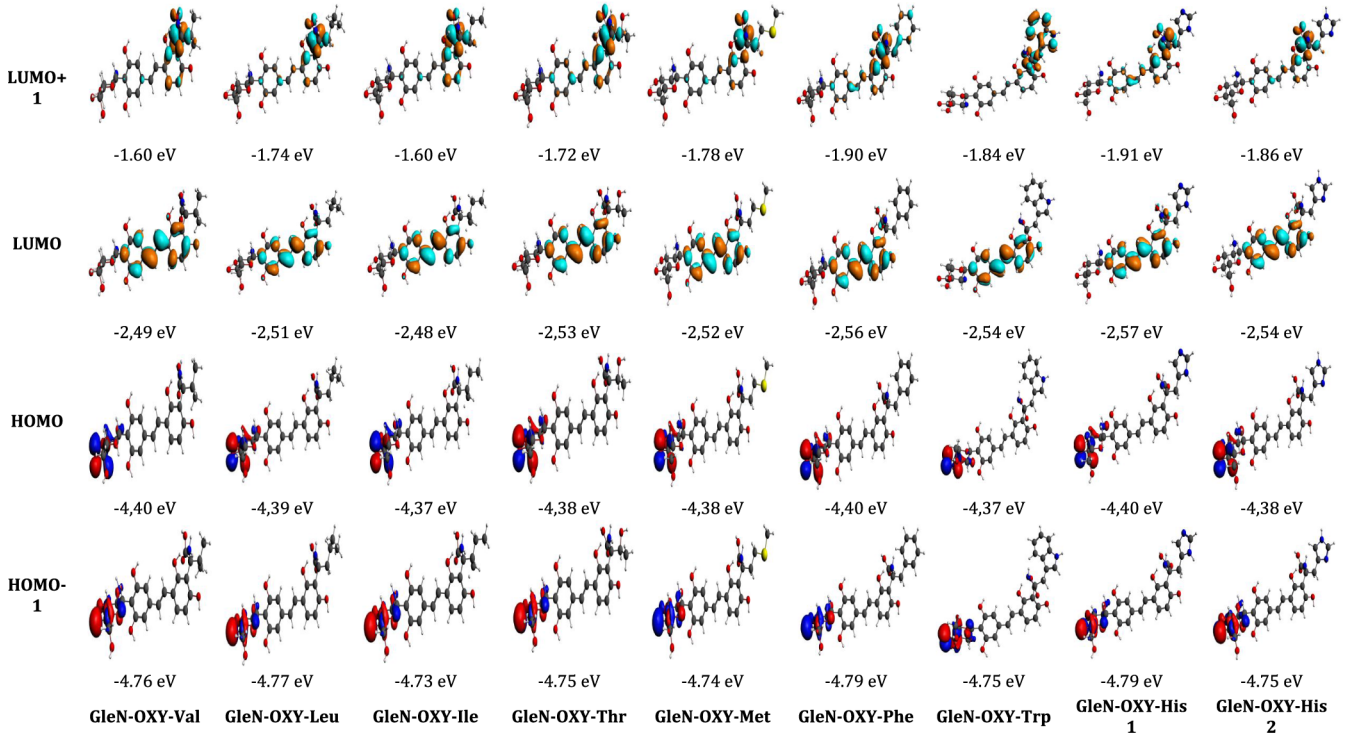

Figure 3. Graphical representation sketched of the four "Gouterman's orbitals" for the target compounds with their energies (eV) indicated (isodensity value 0.03 au).

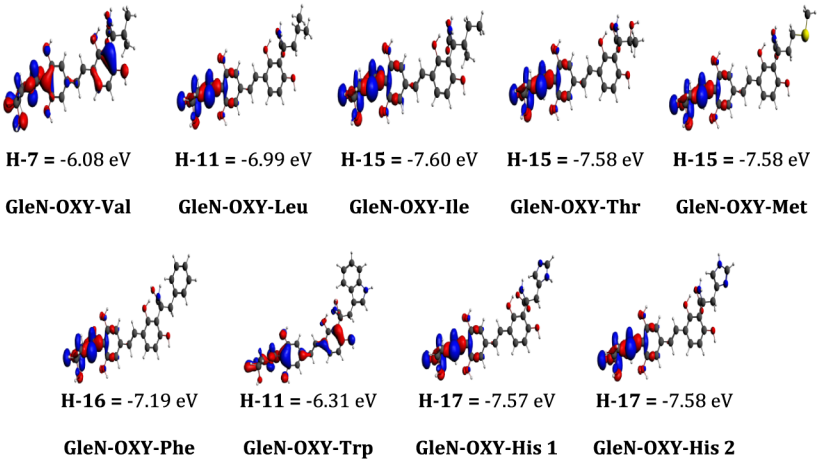

Figure 4. Graphical representation of HOMOs representing covalent recouvrement of target compounds with their energies (eV) indicated (isodensity value 0.03 au).

parameters of the bond critical points (BCRs) and ring critical points (RCPs) discovered for the systems shown in Figure 7. The values of the electron density $\rho(r)$, its Laplacian ($\nabla^2\rho(r)$), and the total energy density of the electrons (H) and its two components: the kinetic electronic energy density (G) and potential (V), calculated at the appropriate RCP and BCR, are reported below (see Table 5).

According to the results of the AIM analysis, Espinosa et al.106 classified atomic interactions into three types:

- Type 1: Pure closed-shell interaction

$$(\rho(r) < 0.07, \nabla^2\rho(r) < 0, H(r) < 0, |V|/G < 1)$$

- Type 2: Intermediate interactions

$$(0.07 < \rho(r) < 0.15, \nabla^2\rho(r) < 0, H(r) < 0, 1 < |V|/G < 2)$$

- Type 3: Pure covalent interaction

$$(\rho(r) < 0.15, \nabla^2\rho(r) < 0, H(r) < 0, |V|/G < 2)$$

To begin with, the results show that GleN-OXY-Ile has eight BCPs, including two intermediate interactions and six closed-shell interactions. GleN-OXY-Trp has eight BCRs: two intermediate interactions, one close to a covalent interaction, and five closed-shell interactions. At the moment, the OXY only has two BCPs of closed-shell interaction type.18

Bader's quantum theory of atoms in molecules (AIM)107 provides a good tool to study the properties of π-electron

https://doi.org/10.1021/acsomega.4c04356
ACS Omega 2024, 9, 37128−37140

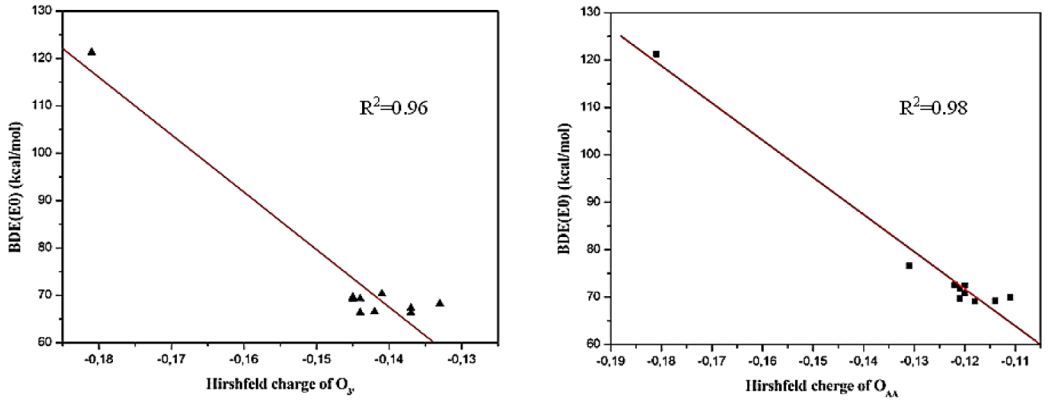

Figure 5. Correlation between BDE(E0) values and Hirshfeld charge of $O_{3'}$ and O_{AA} calculated by DFT.

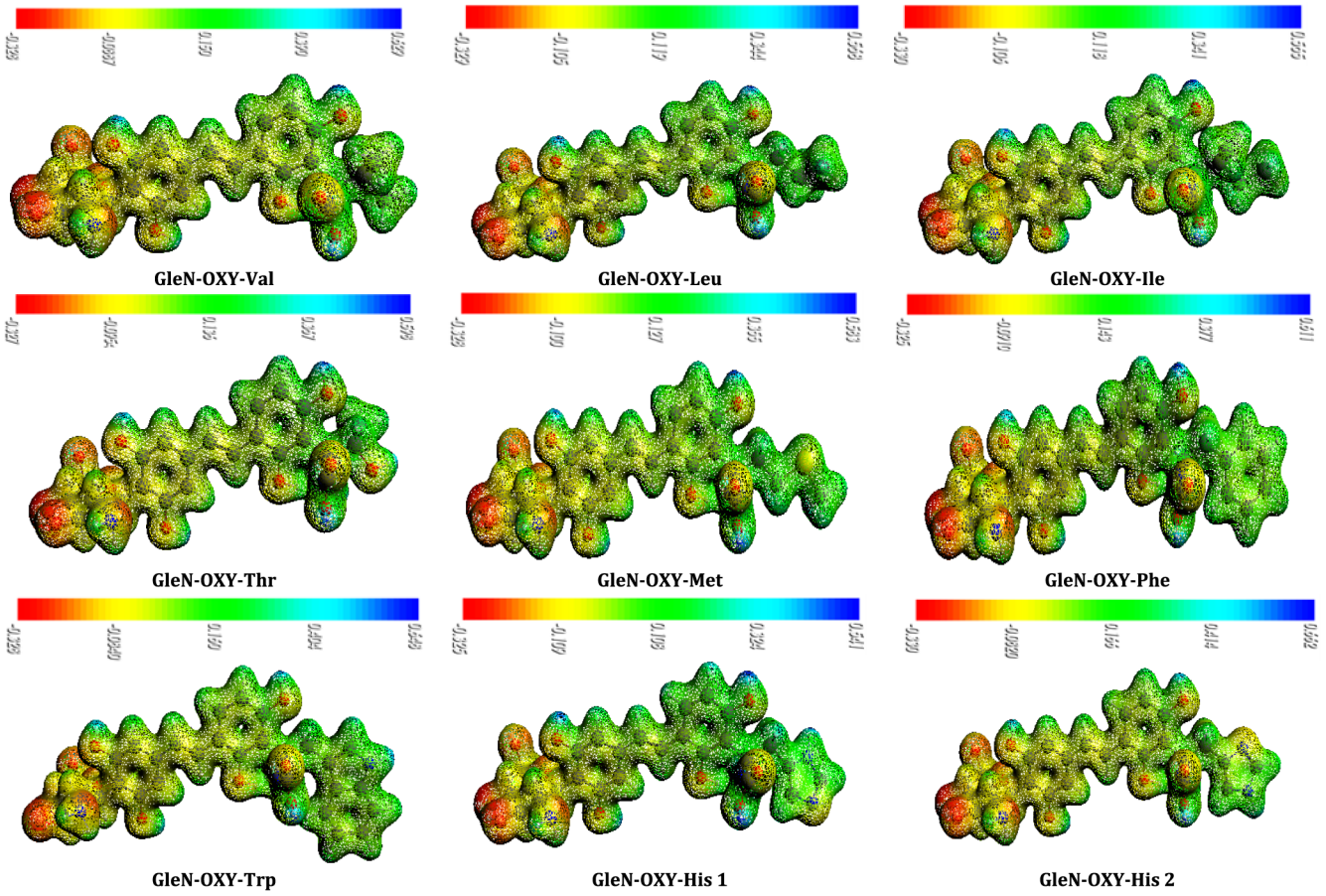

Figure 6. Molecular electrostatic potential (MEP) maps of the optimized structures showing electron density isosurface for all systems (positive MEP = blue, negative MEP = red) (isodensity value 0.03 au).

delocalization of a structure. In the sense of electron density properties estimated at the ring critical point (RCP).[76] A potential new quantitative trait of π electron delocalization was discovered by Palusiak and Krygowski:[108] the total energy density of the electrons H, as well as its component; the kinetic electronic energy density (G). According to the equation:

$$H = G + V \tag{2}$$

The higher the value of H, the greater the delocalization of the π electrons. These results encouraged us to consider the RCPs' estimated AIM parameters to characterize the aromaticity of aromatic rings and aromatic quasi-rings formed by intramolecular hydrogen bonds and which can have an aromatic character.[107−109] The aromaticity of a system positively influences its antioxidant activity; this capacity is closely correlated with the delocalization of π-electrons.[110−113] Hence the more the structure is delocalized, the more stable its radical, anionic, or cationic forms.[98] It has been confirmed that phenyl rings and quasi-rings formed by intramolecular hydrogen bonds can have an aromatic character.[107−109]

The study of the RCPs parameters for all cycles of our two biomaterials, GleN-OXY-Ile and GleN-OXY-Trp, reveals a relationship between the energy densities ρ and H, G, and V. However, a very similar relationship can be discovered for

https://doi.org/10.1021/acsomega.4c04356
ACS Omega 2024, 9, 37128−37140

Table 5. Topological Properties Parameters of the Electron Density Function at BCP and RCP in Phenylic Rings of the Systems in Figure 7[ab]

		BCPs					RCPs						
compounds			$\rho(r)$	$\nabla^2\rho(r)$	H	$\|V\|/G$		$\rho(r)$	$\nabla^2\rho(r)$	H	G	V	$\|V\|/G$
GleN-OXY-Ile	GleN	BCP 1	0.07	0.128	−0.017	1.347	**RCP1**	0.043	0.236	0.001	0.05	−0.049	0.98
		BCP 2	0.015	0.057	0.002	0.836	RCP2	0.023	0.131	0.003	0.022	−0.019	0.863
							RCP3	0.012	0.062	0.002	0.01	−0.007	0.7
	OXY	BCP 3	0.012	0.046	0.001	0.821	RCP4	0.024	0.15	0.004	0.028	−0.024	0.857
		BCP 4	0.011	0.045	0.001	0.803	**RCP5**	0.012	0.055	0.002	0.01	−0.008	0.8
							RCP6	0.012	0.05	0.002	0.01	−0.008	0.8
							RCP7	0.024	0.148	0.004	0.028	−0.024	0.857
	Ile	BCP 5	0.018	0.074	0.002	0.862	**RCP8**	0.012	0.057	0.002	0.01	−0.008	0.8
		BCP 6	0.013	0.053	0.002	0.816	**RCP9**	0.012	0.067	0.002	0.01	−0.008	0.8
		BCP 7	0.103	0.022	−0.049	1.9	**RCP10**	0.027	0.157	0.003	0.03	−0.027	0.9
		BCP 8	0.012	0.046	0.001	0.816	**RCP11**	0.012	0.05	0.002	0.01	−0.008	0.8
GleN-OXY-Trp	GleN	BCP 1	0.07	0.127	−0.017	1.351	**RCP1**	0.043	0.236	0.001	0.052	−0.051	0.98
		BCP 2	0.015	0.06	0.002	0.839	RCP2	0.023	0.1ç31	0.003	0.023	−0.02	0.87
		BCP 3	0.019	0.086	0.002	0.854	**RCP3**	0.012	0.062	0.002	0.01	−0.008	0.8
							RCP4	0.019	0.095	0.003	0.02	−0.017	0.85
	OXY	BCP 4	0.013	0.049	0.001	0.837	RCP5	0.024	0.149	0.004	0.028	−0.027	0.964
							RCP6	0.013	0.061	0.002	0.01	−0.008	0.8
							RCP7	0.024	0.147	0.004	0.028	−0.024	0.857
	Trp	BCP 5	0.023	0.09	0.002	0.896	**RCP8**	0.013	0.073	0.003	0.015	−0.012	0.8
		BCP 6	0.028	0.072	−0.001	1.043	**RCP9**	0.025	0.151	0.004	0.03	−0.026	0.867
		BCP 7	0.011	0.044	0.001	0.785	**RCP10**	0.007	0.025	0.001	0.004	−0.003	0.75
		BCP 8	0.114	−0.009	−0.062	2.039	**RCP11**	0.007	0.034	0.001	0.004	−0.003	0.75
							RCP12	0.01	0.042	0.001	0.004	−0.003	0.778
							RCP13	0.053	0.332	0.002	0.055	−0.053	0.964
							RCP14	0.024	0.151	0.004	0.03	−0.026	0.867

[a]RCP: Ring Critical Point of cycle. [b]RCP: Ring Critical Point of quasi-cycle.

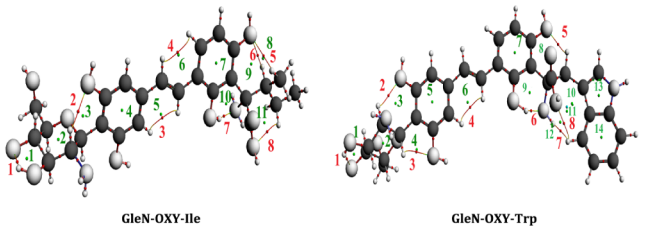

Figure 7. Display illustration of the bond critical points (BCPs in red) and ring critical points (RCPs in green) of GleN-OXY-Ile and GleN-OXY-Trp with AIM analysis.

quasi-cycles. This is consistent with the observations obtained about BCPs. An increase in the electron density at the RCP is accompanied by an increase in the value of H, related to a growing dominance of G over the V term. G values predominate in sections of molecules where the movement of electrons flows more quickly; in other words, where the electrons are less localized. Thus, H's and its constituents' examination in RCP provides valuable information about a given cycle if its aromaticity is taken into account. Considering the primary notions of aromaticity are founded on the occurrence of π-electron delocalization inside the cyclic system, given that the latter is to be the cause of aromatic stability.[114−122]

The highest H values are observed for phenyl rings, implying that electrons are significantly delocalized in the center of these rings. This is consistent with our belief that these ring structures should be classified as aromatic. The H values in bridged rings are significantly lower than those in phenyl rings. Nevertheless, the involvement of the H-bridge within the phenomena of electron delocalization has been perfectly characterized.[122−124]

We also observed GleN in GleN-OXY-Ile and GleN-OXY-Trp, exhibiting an electron delocalization despite its chair shape. The aromatic characteristic of molecules was first identified in planar molecules, and this was related to the planarity of the π-electron system.[108,122,123] But now, in general, it is accepted that aromaticity does not have to be linked to planar molecules. Examples include *para*- and *meta*-cyclophanes.[124−126] The flatness of aromatic compounds can be easily disrupted,[127] due to sufficiently strong intermolecular interactions in the crystal structure; benzene at 20 K in its crystalline form has a chair conformation.[126,127]

Therefore, the AIM results demonstrated that by the appearance of quasi-rings throughout the structure, having significantly high H and notable G (kinetic term) throughout the structure, as well as the rings, proves that the delocalization of π-electrons occurs from one end of the molecule to the other. Thus, this explains the significant antioxidant activity of the grafted geometries, considering that the antioxidant activity is closely correlated with the delocalization of π-electrons.[128−131]

4. CONCLUSIONS

A theoretical investigation was conducted using the PW91/TZP level in water on newly designed biomaterials. These biomaterials involve the grafting of small molecules onto the 3 and 4' carbons of the *trans*-2,4,3′,5′-tetrahydroxystilbene skeleton, specifically the negatively charged D-glucosamine and a series of essential amino acids, which are individually attached through carbon atoms carrying carboxyl and amine

https://doi.org/10.1021/acsomega.4c04356
ACS Omega 2024, 9, 37128−37140

groups. The primary goal of this exploration is to enhance their antioxidant activities post-assembly. The findings from this study are extensive:

- **Structural insights**: All the biomaterials maintain a completely planar structure and preserve the double bonds linking the aromatic rings, which enhances the effects of π-electron conjugation and delocalization compared to the original compounds.
- **Antioxidant activity**: The bond dissociation energy (BDE, E0) quantifies the antioxidant activity. Two candidates, GleN-OXY-Ile and GleN-OXY-Trp, were highlighted with an average BDE (E0) of 66.355 kcal/mol. Their antioxidant activities are 1.82 times greater than *t*-OXY, 2.5 times that of free essential amino acids, and 1.55 times compared to ascorbic acid. The smaller H−L energy gaps in these compounds, 1.82 and 1.83 eV, respectively, indicate a higher reactivity due to easier electron movement from HOMO to LUMO.
- **Quantum calculations and AIM theory**: The use of Bader's quantum theory of atoms in molecules (AIM) suggests that the design of these biomaterials not only retains rings but also encourages the formation of quasi-rings, contributing to their aromaticity and, consequently, their antioxidant activities. The compounds effectively reduce oxidizable species by releasing hydrogen atoms or electrons from sites of lower electronegativity, as estimated by Hirshfeld atomic charges. A correlation between reduced electronegativity and lower BDE was established.
- **Molecular electrostatic potential (MEP)**: MEP mapping indicates that the distribution of negative potential sites is concentrated on the oxygen atoms attached to GleN (sites prone to electrophilic attacks), while positive potential sites are around the hydrogen atoms (H2, H4, H3′, and H5′) of the OXY and the hydrogen of the amino acid's carboxyl group (sites of nucleophilic attacks).
- **Frontier orbital theory**: The theoretical predictions categorize these structures as potent electron acceptors through their OXY and amino acid fragments, indicating their capability to engage in electronic interactions.
- **Charge variations**: There is a notable difference in charge distribution between the free and complexed OXY, indicative of a covalent bond between OXY and the rest of the complex and an ionic bond with the amino acid.

In conclusion, the results from this theoretical investigation suggest that these newly engineered biomaterials, derived from small biodegradable molecules, are promising candidates as high-performance antioxidants. This class of materials is poised to offer significant value in the pharmaceutical field, especially in developing treatments that leverage their enhanced antioxidant properties.

AUTHOR INFORMATION

Corresponding Author

Yacine Benguerba − *Laboratoire de Biopharmacie Et Pharmacotechnie (LBPT), Université Ferhat ABBAS Sétif−1, Sétif 19000, Algeria;* orcid.org/0000-0002-8251-9724; Email: yacinebenguerba@univ-setif.dz

Authors

Salima Hamadouche − *Laboratoire de Chimie des Matériaux et des Vivants: Activité & Réactivité (LCMVAR), Université Batna1, Batna 5000, Algeria*

Hafida Merouani − *Laboratoire de Chimie des Matériaux et des Vivants: Activité & Réactivité (LCMVAR), Université Batna1, Batna 5000, Algeria; Département de Socle Commun, Faculté de Technologie, Université Ben Boulaid Batna 2, Batna 5000, Algeria*

Omaima Aidat − *Laboratory of Food Technology and Nutrition, Abdelhamid Ibn Badis University, Mostaganem 27000, Algeria*

Nadia Ouddai − *Université Batna1, Batna 5000, Algeria*

Barbara Ernst − *Laboratoire de Reconnaissance et Procédés de Séparation Moléculaire (RePSeM), Université de Strasbourg, CNRS, IPHC UMR 7178, Strasbourg F-67000, France*

Manawwer Alam − *Department of Chemistry, College of Science, King Saud University, Riyadh 11451, Saudi Arabia;* orcid.org/0000-0001-9540-8532

Complete contact information is available at: https://pubs.acs.org/10.1021/acsomega.4c04356

Notes

The authors declare no competing financial interest.

ACKNOWLEDGMENTS

We sincerely thank the Algeria's Ministry of Higher Education and Scientific Research for its financial contribution. The authors thank the Researchers Supporting Project (RSP2024R113), King Saud University, Riyadh, Saudi Arabia.

REFERENCES

(1) Manach, C.; et al. Polyphenols: Food sources and bioavailability. *Am. J. Clin. Nutr.* **2004**, *79* (5), 727−747.

(2) Tang, D.-W.; et al. Characterization of tea catechins-loaded nanoparticles prepared from chitosan and an edible polypeptide. *Food Hydrocolloids* **2013**, *30* (1), 33−41.

(3) Denev, P. N.; Kratchanov, C. G.; Ciz, M.; Lojek, A.; Kratchanova, M. G. Bioavailability and Antioxidant Activity of Black Chokeberry(Aronia melanocarpa) Polyphenols: in vitro and in vivo Evidences and Possible Mechanisms of Action: A Review. *Comp Rev Food Sci Food Safe* **2012**, *11* (5), 471−489.

(4) Ensign, L. M.; Cone, R.; Hanes, J. Oral drug delivery with polymeric nanoparticles: gastro-intestinalinal mucus barriers. *Adv. Drug Delivery Rev.* **2012**, *64* (6), 557−570.

(5) Khalifa, I.; et al. Polyphenols of mulberry fruits as multifaceted compounds: Compositions, metabolism, health benefits, and stability—A structural review. *J. Funct. Foods* **2018**, *40*, 28−43.

(6) Xiao, J. Stabilitylity of dietary polyphenols: It's never too late to mend? *Food Chem. Toxicol.* **2018**, *119*, 3−5.

(7) Deng, J. Technological aspects and stability of polyphenols. *Polyphenols: Properties, Recovery, And Applications*; Elsevier, 2018, 295323. .

(8) Benayahoum, A.; et al. Homolytic and heterolytic O−H bond cleavage in trans-resveratrol and some phenantrene analogs: A theoretical study. *Comput. Theor. Chem.* **2014**, *1037*, 1−9.

(9) Lorenz, P.; et al. Oxyresveratrol and resveratrol are potent antioxidants and free radical scavengers: Effect on nitrosative and oxidative stress derived from microglial cells. *Nitric Oxide* **2003**, *9* (2), 64−76.

(10) Likhitwitayawuid, K.; et al. Phenolics With Antiviral Activity From Millettia Erythrocalyx And Artocarpus Lakoocha. *Nat. Prod. Res.* **2005**, *19* (2), 177−182.

(11) Chen, Y.-C.; et al. Morus alba and active compound oxyresveratrol exert anti-inflammatory activity via inhibition of

https://doi.org/10.1021/acsomega.4c04356
ACS Omega 2024, 9, 37128−37140

leukocyte migration involving MEK/ERK signaling. *BMC Complementary Altern. Med.* **2013**, *13*, 45.
(12) Zhang, Z.; et al. Antioxidant Properties Of Ethanolic Extract From Ramulus Mori (Sangzhi). *Food Sci. Technol. Int.* **2009**, *15* (5), 435−444.
(13) Weber, J. T.; et al. Potential neuroprotective effects of oxyresveratrol against traumatic injury. *Eur. J. Pharmacol.* **2012**, *680* (1−3), 55−62.
(14) Rahman, M. A.; et al. Antioxidant compound, oxyresveratrol, inhibits APP production through the AMPK/ULK1/mTOR-mediated autophagy pathway in mouse cortical astrocytes. *Antioxidants* **2021**, *10* (3), 408.
(15) Yang, G.; et al. Inhibitory effects of oxyresveratrol on ERK and Smad1/2 phosphorylation and HSC activation in preventing carbon tetrachloride-induced rat liver fibrosis. *Food Sci. Hum. Wellness* **2021**, *10* (1), 6−12.
(16) Liu, T.; Liu, M.; Guo, Q.; Liu, Y.; Zhao, Y.; Wu, Y.; Sun, B.; Wang, Q.; Liu, J.; Han, J. Investigation of binary and ternary systems of human serum albumin with oxyresveratrol/piceatannol and/or mitoxantrone by multipectroscopy, molecular docking and cytotoxicity evaluation. *J. Mol. Liq* **2020**, *311*, 113364.
(17) Likhitwitayawuid, K. J. M. Oxyresveratrol: Sources, productions, biological activities, pharmacokinetics, and delivery systems. *Molecules* **2021**, *26* (14), 4212.
(18) Hamadouche, S.; et al. Theoretical evaluation of the antioxidant activity of some stilbenes using the Density Functional Theory. *J. Mol. Struct.* **2021**, *1229*, 129496.
(19) Hamadouche, S.; et al. heoretical Exploration Of Enhanced Antioxidant Activity In Copper Complexes Of Tetrahydroxystilbenes: Insights Into Mechanisms And Molecular InteractionsT. *ACS Omega* **2024**, *9*, 9076.
(20) Koga, C. C.; Andrade, J. E.; Ferruzzi, M. G.; Lee, Y. Stability of Trans -Resveratrol Encapsulated in a Protein Matrix Produced Using Spray Drying to UV Light Stress and Simulated Gastro-Intestinal Digestion. *J. Food Sci.* **2016**, *81* (2), C292−C300.
(21) Davidov-Pardo, G. Resveratrol Encapsulation: Designing Delivery Systems To Overcome Solubility, Stability And Bioavailability Issues. *Trends Food Sci. Technol.* **2014**, *38* (2), 88−103.
(22) Akinwumi, B. C.; Bordun, K.-A. M.; Anderson, H. D. Biological activities of stilbenoids. *Int. J. Mol. Sci.* **2018**, *19* (3), 792.
(23) Matencio, A.; Dhakar, N. K.; Bessone, F.; Musso, G.; Cavalli, R.; Dianzani, C.; García-Carmona, F.; López-Nicolás, J. M.; Trotta, F. Study of oxyresveratrol complexes with insoluble cyclodextrin based nanosponges: Developing a novel way to obtain their complexation constants and application in an anticancer study. *Carbohydr. Polym.* **2020**, *231*, 115763.
(24) Gaglio, S. C.; et al. Oxyresveratrol inhibits R848-induced pro-inflammatory mediators release by human dendritic cells even when embedded in PLGA nanoparticles. *Molecules* **2021**, *26* (8), 2106.
(25) Han, H. S.; Koo, S. Y.; Choi, K. Y. Emerging nanoformulation strategies for phytocompounds and applications from drug delivery to phototherapy to imaging. *Bioact. Mater.* **2022**, *14*, 182−205.
(26) Nugraha, M. W.; Iswandana, R.; Jufri, M. Preparation, characterization, and formulation of solid lipid nanoparticles lotion from mulberry roots (Morus alba L.). Appl. *Int. J. Appl. Pharm.* **2020**, *12*, 182−186.
(27) Donini, M.; et al. Oxyresveratrol-loaded PLGA nanoparticles inhibit oxygen free radical production by human monocytes: Role in nanoparticle biocompatibility. *Molecules* **2021**, *26* (14), 4351.
(28) Dhakar, N. K.; et al. Comparative evaluation of solubility, cytotoxicity and photostability studies of resveratrol and oxyresveratrol loaded nanosponges. *Pharmaceutics* **2019**, *11* (10), 545.
(29) Palmer, L. C.; Stupp, S. I. Molecular Self-Assembly Into One-Dimensional Nanostructures. *Acc. Chem. Res.* **2008**, *41* (12), 1674−1684.
(30) Kubik, S. Amino acid containing anion receptors. *Chem. Soc. Rev* **2009**, *38* (2), 585−605.
(31) Matson, J. B.; et al. Peptide self-assembly for crafting functional biological materials. *Curr. Opin. Solid State Mater. Sci.* **2011**, *15* (6), 225−235.
(32) Wu, G. Amino Acids: metabolism, Functions, And Nutrition. *Amino Acids* **2009**, *37*, 1−17.
(33) Lourenco, R.; Camilo, M. E. Taurine: A conditionally essential amino acid in humans? An overview in health and disease. *Nutr. Hosp.* **2002**, *17* (6), 262−270.
(34) Reeds, P. J. Dispensable and indispensable amino acids for humans. *J. Nutr.* **2000**, *130* (7), 1835S−1840S.
(35) Xu, N.; Chen, G.; Liu, H. J. M. Antioxidative categorization of twenty amino acids based on experimental evaluation. *Molecules* **2017**, *22* (12), 2066.
(36) Torkova, A.; et al. Structure-functional study of tyrosine and methionine dipeptides: an approach to antioxidant activity prediction. *Int. J. Mol. Sci.* **2015**, *16* (10), 25353−25376.
(37) Peña-Ramos, E. A.; et al. Fractionation and characterisation for antioxidant activity of hydrolysed whey protein. *J. Sci. Food Agric.* **2004**, *84* (14), 1908−1918.
(38) Wu, H.-C.; Chen, H.-M.; Shiau, C.-Y. Free amino acids and peptides as related to antioxidant properties in protein hydrolysates of mackerel (Scomber austriasicus). *Food Res. Int.* **2003**, *36* (9−10), 949−957.
(39) Pérez, R. A.; et al. Amino acid composition and antioxidant capacity of Spanish honeys. *J. Agric. Food Chem.* **2007**, *55* (2), 360−365.
(40) World Health Organization. *Guideline: Sugars intake for adults and children*; World Health Organization, 2015.
(41) Arnone, D.; Chabot, C.; Heba, A.-C.; Kökten, T.; Caron, B.; Hansmannel, F.; Dreumont, N.; Ananthakrishnan, A. N.; Quilliot, D.; Peyrin-Biroulet, L.; et al. Sugars and gastrointestinal health. *Clin. Gastroenterol. Hepatol.* **2022**, *20* (9), 1912−1924.e7.
(42) Fu, X.; et al. Targeted delivery of Fenton reaction packages and drugs for cancer theranostics. *Appl. Mater. Today* **2022**, *26*, 101353.
(43) Sal'nikova, S.; Drogovoz, S.; Zupanets, I. A. Liver-Protective Properties Of D-Glucosamine. *Farmakol. Toksikol.* **1990**, *53* (4), 33−35.
(44) McCarty, M. F. Glucosamine For Wound Healing. *Med. Hypotheses* **1996**, *47* (4), 273−275.
(45) Lippiello, L. Glucosamine and chondroitin sulfate: biological response modifiers of chondrocytes under simulated conditions of joint stress. *Osteoarthritis Cartilage* **2003**, *11* (5), 335−342.
(46) Gupta, K. C.; Kumar, M. N. V. An overview on chitin and chitosan applications with an emphasis on controlled drug release formulations. *J. Macromol. Sci., Polym. Rev.* **2000**, *40* (4), 273−308.
(47) Miao, Q.; et al. Preparation, Anticoagulant and Antioxidant Properties of Glucosamine-Heparin Salt. *Mar. Drugs* **2022**, *20* (10), 646.
(48) Xu, S.; et al. Antioxidant activity in vitro and in vivo of the polysaccharides from different varieties of Auricularia auricula. *Food Funct.* **2016**, *7* (9), 3868−3879.
(49) Sun, T.; et al. Preparation of chitosan oligomers and their antioxidant activity. *Eur. Food Res. Technol.* **2007**, *225*, 451−456.
(50) Abd El-Hack, M. E.; et al. Antimicrobial and antioxidant properties of chitosan and its derivatives and their applications: A review. *Int. J. Biol. Macromol.* **2020**, *164*, 2726−2744.
(51) Kumar, S.; Koh, J. Physiochemical, optical and biological activity of chitosan-chromone derivative for biomedical applications. *IJMS* **2012**, *13* (5), 6102−6116.
(52) Varma, A.; Deshpande, S.; Kennedy, J. F. Metal Complexation By Chitosan And Its Derivatives: A Review. *Carbohydr. Polym.* **2004**, *55* (1), 77−93.
(53) Rinaudo, M. Chitin And Chitosan: properties And Applications. *Prog. Polym. Sci.* **2006**, *31* (7), 603−632.
(54) Jeuniaux, C.; et al. Chitosan as a tool for the purification of waters. *Chitin Nat. Technol.* **1986**, 551−570.
(55) Hirano, S.; et al. Chitosan as an ingredient for domestic animal feeds. *J. Agric. Food Chem.* **1990**, *38* (5), 1214−1217.

https://doi.org/10.1021/acsomega.4c04356
ACS Omega 2024, 9, 37128−37140

(56) Abdel-Hafez, S. M.; Zapp, J.; Gallei, M.; Schneider, M. Formulation attributes, acid tunable degradability and cellular interaction of acetalated maltodextrin nanoparticles. *Carbohydrate polymers* **2022**, *288*, 119378.
(57) Barclay, T. G.; et al. Review of polysaccharide particle-based functional drug delivery. *Carbohydr. Polym.* **2019**, *221*, 94−112.
(58) Bhattacharya, A.; Misra, B. N. Graftingting: A Versatile Means To Modify Polymers: Techniques, Factors And Applications. *Prog. Polym. Sci.* **2004**, *29* (8), 767−814.
(59) Spizzirri, U. G.; et al. Synthesis of antioxidant polymers by grafting of gallic acid and catechin on gelatin. *Biomacromolecules* **2009**, *10* (7), 1923−1930.
(60) Sharma, K.; Kadian, V.; Kumar, A.; Mahant, S.; Rao, R. Evaluation of solubility, photostability and antioxidant activity of ellagic acid cyclodextrin nanosponges fabricated by melt method and microwave-assisted synthesis. *J. Food Sci. Technol.* **2022**, *59*, 898−908.
(61) Ihara, N.; et al. Amplification of inhibitory activity of catechin against disease-related enzymes by conjugation on poly (ε-lysine). *Biomacromolecules* **2004**, *5* (5), 1633−1636.
(62) Brzonova, I.; et al. Enzymatic synthesis of catechol and hydroxyl-carboxic acid functionalized chitosan microspheres for iron overload therapy. *Eur. J. Pharm. Biopharm.* **2011**, *79* (2), 294−303.
(63) Jeon, Y. O.; et al. Improving solubility, stability, and cellular uptake of resveratrol by nanoencapsulation with chitosan and γ-poly (glutamic acid). *Colloids Surfaces B Biointerfaces* **2016**, *147*, 224−233.
(64) Chung, J. H.; et al. Resveratrol-loaded chitosan−γ-poly (glutamic acid) nanoparticles: Optimization, solubility, UV stability, and cellular antioxidant activity. *Colloids Surfaces B Biointerfaces* **2020**, *186*, 110702.
(65) Prodpran, T.; Benjakul, S.; Phatcharat, S. Effect of phenolic compounds on protein cross-linking and properties of film from fish myofibrillar protein. *Int. J. Biol. Macromol.* **2012**, *51* (5), 774−782.
(66) Aewsiri, T.; et al. Antioxidative activity and emulsifying properties of cuttlefish skin gelatin modified by oxidised phenolic compounds. *Food Chem.* **2009**, *117* (1), 160−168.
(67) Drzėdon, J.; Pawlak, M.; Matyka, N.; Sikorski, A.; Gawdzik, B.; Jacewicz, D. Relationship between Antioxidant Activity and Ligand Basicity in the Dipicolinate Series of Oxovanadium(IV) and Dioxovanadium(V) Complexes. *IJMS* **2021**, *22* (18), 9886.
(68) Shao, Y.; et al. Evaluation of chitosan−anionic polymers based tablets for extended-release of highly water-soluble drugs. *Asian J. Pharm. Sci.* **2015**, *10* (1), 24−30.
(69) Te Velde, G. T.; et al. Chemistry with ADF. *J. Comput. Chem.* **2001**, *22* (9), 931−967.
(70) Boerrigter, P.; et al. Three-dimensional numerical integration for electronic structure calculations. *Int. J. Quantum Chem.* **1988**, *33* (2), 87−113.
(71) Aprà, E.; Fortunelli, A. Density-functional study of Pt13 and Pt55 cuboctahedral clusters. *J. Mol. Struct.* **2000**, *501*, 251−259.
(72) Versluis, L.; Ziegler, T. The determination of molecular structures by density functional theory. The evaluation of analytical energy gradients by numerical integration. *J. Chem. Phys.* **1988**, *88* (1), 322−328.
(73) Pye, C. C.; Ziegler, T. An implementation of the conductor-like screening model of solvation within the Amsterdam density functional package. *Theor. Chem. Acc.* **1999**, *101*, 396−408.
(74) Ounissi, A.; et al. Theoretical investigation on structural and physicochemical properties of some ionic liquids. *Comput. Theor. Chem.* **2016**, *1092*, 68−73.
(75) Bader, R. F. W. *Atoms in Molecules: A Quantum Theory*; Clarendon Press, 1990.
(76) Howard, S.; Krygowski, T. M. Benzenoid hydrocarbon aromaticity in terms of charge density descriptors. *Can. J. Chem.* **1997**, *75* (9), 1174−1181.
(77) Baranov, A. I.; Kohout, M. Topological analysis of real space properties for the solid-state full-potential APW DFT method. *J. Phys. Chem. Solids* **2010**, *71* (9), 1350−1356.
(78) Aguamah, G. E.; Langcake, P.; Leworthy, D. P.; Page, J. A.; Pryce, R. J.; Strange, R. N. Two novel stilbene phytoalexins from Arachis hypogaea. *Phytochemistry* **1981**, *20*, 1381−1383.
(79) Sobolev, V. S.; Cole, R. J. Trans-resveratrol content in commercial peanuts and peanut products. *J. Agric. Food Chem.* **1999**, *47* (4), 1435−1439.
(80) Condori, J.; et al. Induced biosynthesis of resveratrol and the prenylated stilbenoids arachidin-1 and arachidin-3 in hairy root cultures of peanut: Effects of culture medium and growth stage. *Plant Physiol. Biochem.* **2010**, *48* (5), 310−318.
(81) Pourjavadi, A.; Fatahi, A.; Kurdtabar, M.; et al. DFT/B3LYP Study Of Thermochemistry Of D-Glucosamine, a Representative Polyfunctional Bioorganic Compound. *Scientia Iranica* **2008**, *15*, 4.
(82) Rahmawati, S.; Radiman, C. L.; Martoprawiro, M. A. *Ab Initio* Study of Proton Transfer and Hydration in Phosphorylated Nata de Coco. *Indones. J. Chem.* **2017**, *17* (3), 523−530.
(83) Foster, J. P.; Weinhold, F. Natural hybrid orbitals. *J. Am. Chem. Soc.* **1980**, *102* (24), 7211−7218.
(84) Reed, A. E.; Weinhold, F. Natural localized molecular orbitals. *J. Chem. Phys.* **1985**, *83* (4), 1736−1740.
(85) Reed, A. E.; Curtiss, L. A.; Weinhold, F. Intermolecular interactions from a natural bond orbital, donor-acceptor viewpoint. *Chem. Rev.* **1988**, *88* (6), 899−926.
(86) Chocholoušová, J.; Špirko, V.; Hobza, P. First local minimum of the formic acid dimer exhibits simultaneously red-shifted O−H··· O and improper blue-shifted C−H··· O hydrogen bonds. *Phys. Chem. Chem. Phys.* **2004**, *6* (1), 37−41.
(87) Ahsan, S. M.; et al. Chitosan as biomaterial in drug delivery and tissue engineering. *Int. J. Biol. Macromol.* **2018**, *110*, 97−109.
(88) Siahaan, P.; et al. The validation of molecular interaction among dimer chitosan with urea and creatinine using density functional theory: In application for hemodyalisis membrane. *Int. J. Biol. Macromol.* **2021**, *168*, 339−349.
(89) Jeffrey, G. A.; Saenger, W. *Hydrogen bonding in biological structures*; Springer Science & Business Media, 2012.
(90) Putri, A. D.; et al. Computational studies on the molecular insights of aptamer induced poly (N-isopropylacrylamide)-graft-graphene oxide for on/off-switchable whole-cell cancer diagnostics. *Sci. Rep.* **2019**, *9* (1), 7873.
(91) Amalanathan, M.; Joe, I. H.; Rastogi, V. K. Molecular structure, vibrational spectra and nonlinear optical properties of L-valine hydrobromide: DFT study. *J. Mol. Struct.* **2011**, *985* (1), 48−56.
(92) Burley, S. K.; et al. Molecular structure of leucine amino-peptidase at 2.7-A resolution. *Proc. Natl. Acad. Sci. U. S. A.* **1990**, *87* (17), 6878−6882.
(93) Takano, K.; et al. Contribution of hydrophobic residues to the stability of human lysozyme: calorimetric studies and X-ray structural analysis of the five isoleucine to valine mutants. *J. Mol. Biol.* **1995**, *254* (1), 62−76.
(94) Feyer, V.; et al. Core level study of alanine and threonine. *J. Phys. Chem. A* **2008**, *112* (34), 7806−7815.
(95) Trujillo, J.; et al. X-ray crystallographic study of boroxazolidones obtained from L-ornithine, L-methionine, kainic acid and 2, 6-pyridinedicarboxylic acid. *J. Organomet. Chem.* **1998**, *571* (1), 21−29.
(96) Hiyama, Y.; et al. Molecular structure and dynamics of crystalline p-fluoro-D, L-phenylalanine. A combined x-ray/NMR investigation. *J. Am. Chem. Soc.* **1986**, *108* (10), 2715−2723.
(97) Williams, S.; et al. X-ray crystal structure of the liver X receptor β ligand binding domain: Regulation by a histidine-tryptophan switch. *J. Biol. Chem.* **2003**, *278* (29), 27138−27143.
(98) Mazzone, G.; et al. Antioxidant properties comparative study of natural hydroxycinnamic acids and structurally modified derivatives: Computational insights. *Comput. Theor. Chem.* **2016**, *1077*, 39−47.
(99) Chavarria, D.; et al. Exploring cinnamic acid scaffold: development of promising neuroprotective lipophilic antioxidants. *MedChemcomm* **2015**, *6* (6), 1043−1053.
(100) Queiroz, A. N.; et al. A theoretical antioxidant pharmacophore for resveratrol. *Eur. J. Med. Chem.* **2009**, *44* (4), 1644−1649.

https://doi.org/10.1021/acsomega.4c04356
ACS Omega 2024, 9, 37128−37140

(101) Honório, K. M.; Da Silva, A. B. F. An AM1 study on the electron-donating and electron-accepting character of biomolecules. *Int. J. Quantum Chem.* **2003**, *95* (2), 126−132.
(102) Lewis, D.; Ioannides, C.; Parke, D. J. X. Interaction of a series of nitriles with the alcohol-inducible isoform of P450: Computer analysis of structure—activity relationships. *Xenobiotica* **1994**, *24* (5), 401−408.
(103) Houas, N.; et al. Synthesis, characterization, DFT study and antioxidant activity of (2-hydroxynaphthalen-1-yl) methyl 2-hydroxyphenyl amino phosphonic acid. *J. Mol. Struct.* **2022**, *1247*, 131322.
(104) Al-Janabi, A. S.; et al. New dual inhibitors of SARS-CoV-2 based on metal complexes with Schiff-base 4-chloro-3-methyl phenyl hydrazine: Synthesis, DFT, antibacterial properties and molecular docking studies. *Inorganics* **2023**, *11* (2), 63.
(105) Awad, M. K.; et al. Molecular docking, molecular modeling, vibrational and biological studies of some new heterocyclic α-aminophosphonates. *Spectrochim. Acta, Part A* **2019**, *206*, 78−88.
(106) Espinosa, E.; et al. Topological analysis of the electron density in hydrogen bonds. *Acta Crystallogr., Sect. B: Struct. Sci.* **1999**, *55* (4), 563−572.
(107) Bader, R. F. W. Comment on: Revisiting the variational nature of the quantum theory of atoms in molecules. *Chem. Phys. Lett.* **2006**, *426* (1−3), 226−228.
(108) Palusiak, M.; Krygowski, T. M. Application of AIM Parameters at Ring Critical Points for Estimation of π-Electron Delocalization in Six-Membered Aromatic and Quasi-Aromatic Rings. *Chem.—Euro. J.* **2007**, *13* (28), 7996−8006.
(109) Krygowski, T. M.; et al. Aromaticity from the viewpoint of molecular geometry: application to planar systems. *Chem. Rev.* **2014**, *114* (12), 6383−6422.
(110) Krygowski, T. M.; Szatylowicz, H. Aromaticity: What does it mean? *ChemTexts* **2015**, *1*, 12.
(111) Ali, H. M.; Ali, I. H. A DFT and QSAR study of the role of hydroxyl group, charge and unpaired-electron distribution in anthocyanidin radical stabilization and antioxidant activity. *Med. Chem. Res.* **2017**, *26*, 2666−2674.
(112) van Acker, S. A.; et al. A quantum chemical explanation of the antioxidant activity of flavonoids. *Chem. Res. Toxicol.* **1996**, *9* (8), 1305−1312.
(113) Almeida-Neto, F. W. Q.; et al. Characterization of the structural, spectroscopic, nonlinear optical, electronic properties and antioxidant activity of the N-{4'-[(E)-3-(Fluorophenyl)-1-(phenyl)-prop-2-en-1-one]}-acetamide. *J. Mol. Struct.* **2020**, *1220*, 128765.
(114) Urbaniak, A.; et al. Theoretical investigation of stereochemistry and solvent influence on antioxidant activity of ferulic acid. *Comput. Theor. Chem.* **2013**, *1012*, 33−40.
(115) Jug, K.; Hiberty, P. C.; Shaik, S. σ− π Energy separation in modern electronic theory for ground states of conjugated systems. *Chem. Rev.* **2001**, *101* (5), 1477−1500.
(116) Jug, K.; Koester, A. M. Influence of.sigma. and.pi. electrons on aromaticity. *J. Am. Chem. Soc.* **1990**, *112* (19), 6772−6777.
(117) Hiberty, P. C.; et al. Is the delocalized. pi. system of benzene a stable electronic system? *J. Org. Chem.* **1985**, *50* (23), 4657−4659.
(118) Longuet-Higgins, H. C.; Salem, L. The alternation of bond lengths in long conjugated chain molecules. *Proc. R. Soc. London, Ser. A* **1959**, *251* (1265), 172−185.
(119) Coulson, C.; Dixon, W. T. Bond lengths in cyclic polyenes C2nH2n a re-examination from the valence-bond point of view. *Tetrahedron* **1962**, *17* (3−4), 215−228.
(120) Epiotis, N. D. Bond-deficient molecules. *J. Am. Chem. Soc.* **1984**, *106* (11), 3170−3174.
(121) Shaik, S.; et al. A different story of benzene. *J. Mol. Struct.* **1997**, *398*, 155−167.
(122) Maksić, Z. B.; Barić, D.; Petanjek, I. On the correlation energy of π-electrons in planar hydrocarbons. *J. Phys. Chem. A* **2000**, *104* (46), 10873−10881.
(123) Palusiak, M.; Simon, S.; Solà, M. Interplay between intramolecular resonance-assisted hydrogen bonding and aromaticity in o-hydroxyaryl aldehydes. *J. Org. Chem.* **2006**, *71* (14), 5241−5248.
(124) Gilli, G.; et al. Evidence for resonance-assisted hydrogen bonding from crystal-structure correlations on the enol form of the. beta.-diketone fragment. *J. Am. Chem. Soc.* **1989**, *111* (3), 1023−1028.
(125) Verhoeven, J. W. *The Chemistry of Enols. Zvi Rappoport, ed. John Wiley & Sons, Chichester, 1990. XVI+ 823 pp.,£ 195.00. ISBN 0−471−91720−6*; Wiley Online Library, 1991.
(126) Müller, E. *Neuere Anschauungen der organischen Chemie: Organische Chemie für Fortgeschrittene*; Springer-Verlag, 2013.
(127) Müller, E.. Konstitution Und Farbe. In *Neuere Anschauungen der Organismen Chemie*; Springer, 1940; pp 349374. DOI: .
(128) Jenneskens, L. W.; et al. Molekülstruktur von 8, 11-Dichlor [5] metacyclophan: Ein stark verbogener Benzolring. *Angew. Chem.* **1984**, *96* (3), 236−237.
(129) Krygowski, T.; et al. Aromaticity: A theoretical concept of immense practical importance. *Tetrahedron* **2000**, *56* (13), 1783−1796.
(130) Dijkstra, F.; Van Lenthe, J. H. Aromaticity of bent benzene rings: A VBSCF study. *Int. J. Quant. Chem.* **1999**, *74* (2), 213−221.
(131) Ruble, J.; Galvao, A. Electrostatic potentials from charge-density studies of benzamide at 123 K. *Acta Crystallogr., Sect. B: Struct. Sci.* **1995**, *51* (5), 835−838.

https://doi.org/10.1021/acsomega.4c04356
ACS Omega 2024, 9, 37128−37140